JOURNAL OF MATERIALS SCIENCE 31 (1996) 1367–1373

Processing effect on structural changes of high acid-catalysed silica gel

B. I. LEE*, KUOTUNG CHOU
Department of Ceramic Engineering, Clemson University, Clemson, SC 29634-0907, USA

The structure of silica gels prepared by hydrolysis of tetraethoxysilane (TEOS) with high acid content has been investigated. The gels were obtained by varying the nitric acid contents at a constant H_2O/TEOS molar ratio of 10. The molar compositions were TEOS: H_2O:HNO_3 = 1:10: x (x = 0.1–1.0). The effects of acid content and drying temperature on structural changes in the gels were examined. In addition, the surface area, pore volume, pore size distribution, and the microstructure were determined. The results showed that the pore structure changed to larger pore sizes and broader size distributions as a result of increasing the drying temperature. However, at a constant drying temperature, a higher acid content yielded a higher pore volume. The gels dried at lower temperatures had slit-shaped micropores and a narrow pore size distribution; whereas, the gels dried at higher temperatures had ink bottle-shaped pores and a relatively broad size distribution.

1. Introduction

Production of glasses with tailored properties through the sol–gel method depends significantly on the conditions used during hydrolysis of the metal alkoxide precursors [1, 2]. For silica gels prepared from tetraethoxysilane (TEOS), the hydrolytic polycondensation reactions take place with the functionality of four, hence three-dimensional polymer molecules are generated to form an oxide network. The factors affecting the reactions determine the size of the primary particles of the sol, the gel microstructure, and the formation of crack-free gels.

Among the various hydrolysis conditions, acid content and drying temperature have been identified as two key parameters affecting the properties of the gel. These two factors have a profound influence on the structure development of the dried gels [3, 4]. Yasumori *et al.* [4] showed that the surface areas of xerogels dried at 60 °C were always 50% higher than the gels dried at 30 °C, regardless of the ageing time. In addition, the tendency of the monolithic gels to crack during drying depends on the structural properties with respect to pore shape and pore size distribution [5–8]. Hench [8] ascribed the use of formamide and oxalic acid to reduce the pore size distribution. This was explained as decreasing the magnitude of capillary differential stress during the drying and improved the crack-free integrity of gels. In this study, the pore shape, pore size distribution, and microstructure of TEOS gels are reported as a function of nitric acid content and drying temperature.

2. Experimental procedure

2.1. Gel preparation

The starting materials included TEOS, nitric acid, and distilled water. The sol was formed by hydrolysis of TEOS in distilled water, containing the nitric acid catalyst, and keeping the H_2O/TEOS molar ratio constant at 10. The mixture was stirred at room temperature at two different stirring rates by a magnetic stirrer; the high mixing rate at ~ 600 r.p.m. and low mixing rate at ~ 280 r.p.m. The detailed experimental conditions have been presented in our previous paper [9].

After the hydrolysis the sol was cast into plastic containers, covered with plastic wrap sheets and gelled at 60 °C. The wet gels were subject to ageing in freshly added distilled water for one day. They were dried in the presence of the ageing water at the same temperature as the gelling temperature in an open condition. However, the seals were broken but the covers were kept on for the gels drying at 120 °C. For a comparison, a "basic gel" was also prepared by ageing the wet gel having same acid content in an aqueous ammonia solution with pH 10.

2.2. Gel characterization

Nitrogen adsorption isotherms were obtained by using Quantachrome's Quantasorb. The pore size distributions were calculated by using the desorption isotherm. The specific surface areas were determined by measuring the slope from V–t plot (adsorption volume versus film thickness) [10]. All gel samples were heated at 140 °C and degassed under nitrogen flow prior to analysis.

The structural changes of the gels due to a change in temperature were measured by IR diffuse reflectance spectroscopy using a Perkin-Elmer Model 1600 Fourier Transform Infrared Spectrophotometer. The dried gels were heat-treated in a quartz tube at 200,

* Author to whom correspondence should be addressed.

0022–2461

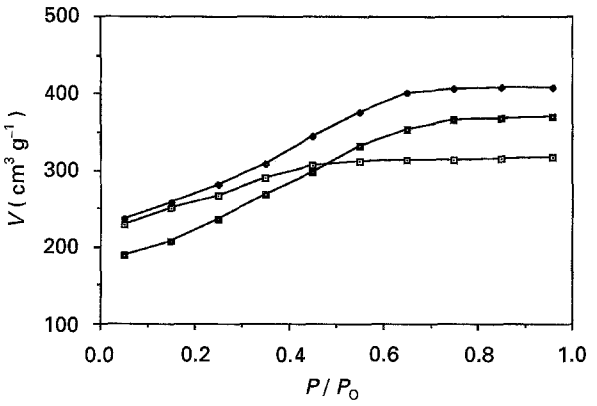

Figure 1 Nitrogen adsorption isotherms of gels prepared with a H_2O/TEOS ratio of 10, HNO_3/TEOS ratios of 0.4 and 1.0 and 1.0 (opaque) and all dried at 60 °C. Key: -□- 0.4/60; -◆- 1.0/60; -■- 1.0/60 (opaque).

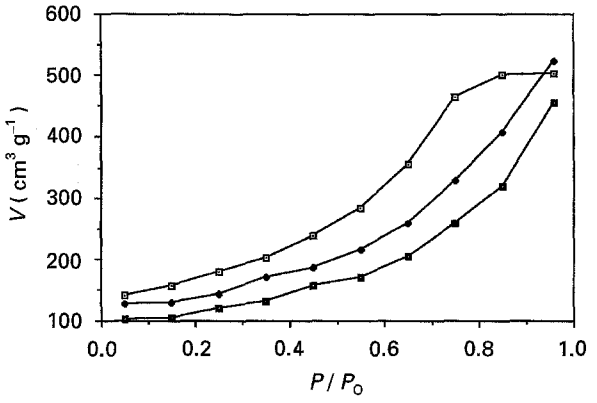

Figure 2 Nitrogen adsorption isotherms of gels prepared with a H_2O/TEOS ratio of 10, HNO_3/TEOS ratios of 0.4 and 1.0, dried at 120 °C; 0.4 (basic gel), dried at 60 °C. Key: -□- 0.4/120; -◆- 1.0/120; -■- 0.4/60 (basic gel).

400, 600 and 700 °C in air for 2 h with 0.85 °C min^{-1} heating rate.

The microstructures of heat-treated gels were observed with JEOL JSM-IC 848 scanning electron microscope. A fractured surface was sputtered with gold to observe the microstructure.

3. Results

3.1. Nitrogen adsorption isotherms

The nitrogen adsorption isotherms (adsorption volume versus relative pressure) on gels with different acid contents and drying temperatures are presented in Figs 1 and 2. The isotherms for the gels dried at 60 °C with HNO_3/TEOS molar ratios (R_a) of 0.4 and 1.0 (denoted as 0.4/60 and 1.0/60) are shown in Fig. 1. The isotherms for gels dried at 120 °C with molar ratios of 0.4 and 1.0 (denoted as 0.4/120 and 1.0/120) are shown in Fig. 2. The adsorption isotherms for 0.4/60, 1.0/60 and 1.0/60 (opaque) gels are shown to be type I of Brunauer's classification [11]. The adsorption isotherm for the 0.4/120 gel is shown to be type IV. The basic gel, as well as 1.0/120, are type II.

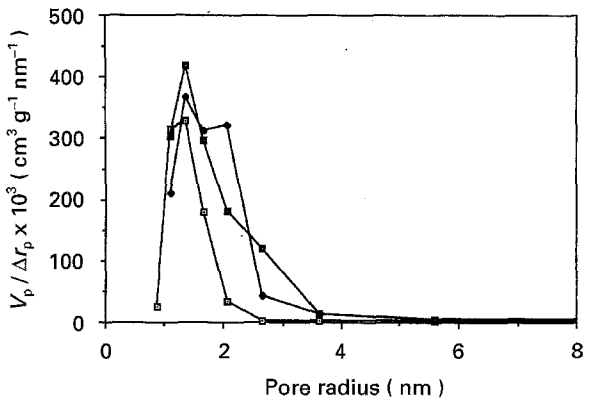

Figure 3 Pore size distribution of gels prepared with a H_2O/TEOS ratio of 10 and HNO_3/TEOS ratios of 0.4 and 1.0 and 1.0 (opaque), dried at 60 °C. Key: -□- 0.4/60; -◆- 1.0/60; -■- 1.0/60 (opaque).

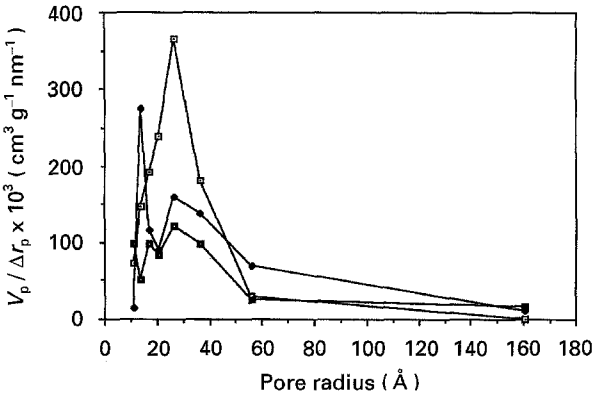

Figure 4 Pore size distribution of gels prepared with a H_2O/TEOS ratio of 10 and HNO_3/TEOS ratios of 0.4 and 1.0, dried at 120 °C; and 0.4 (basic gel), dried at 60 °C. Key: -□- 0.4/120; -◆- 1.0/120; -■- 0.4/60 (basic gel).

3.2. Pore size distribution

Pore size distributions for the gels of 0.4/60, 1.0/60, 0.4/120 and 1.0/120 are shown in Figs 3 and 4, respectively. The pore size distributions become broader in an ascending order of 0.4/60 < 1.0/60 < 0.4/120 < 1.0/120. Comparison of drying temperatures indicates that the average pore diameter is larger and pore size distribution is broader for the gels dried at 120 °C than the gels dried at 60 °C. The gels dried at 120 °C contain pores as large as 16 nm whereas the gels dried at 60 °C contain no pores exceeding 6 nm. The average pore size is 1.5 nm for the gel dried at 60 °C and 3 nm for the gel dried at 120 °C. The pore size distributions appear very narrow for the 0.4/60 (Fig. 3) and 0.4/120 gel (Fig. 4), indicating a rather uniform pore structure. However, broad pore size distributions are shown for the 1.0/60 gel (Fig. 3) and 1.0/120 gel (Fig. 4).

By varying the mixing or stirring rate, different gel morphologies were observed. At the lower mixing rate, the *in situ* formed particles were incorporated in the gels causing opaque appearance of the gels. However, transparent gels were obtained at the higher mixing rate from the same composition of sol. To show the effect of the particles on the structure of the dried gel, a comparison of pore size distribution curves with these gels is given in Fig. 3. There are no obvious

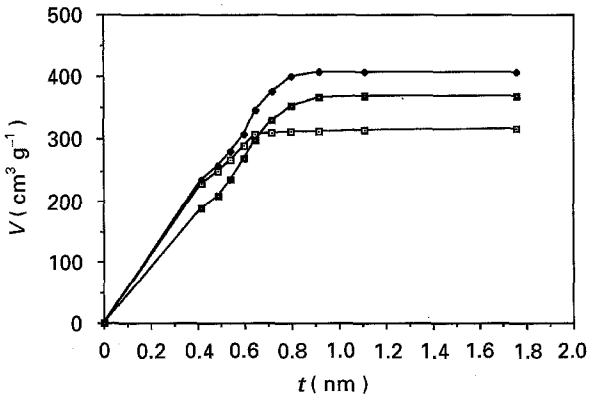

Figure 5 V–t plot of gels prepared with a H_2O/TEOS ratio of 10 and HNO_3/TEOS ratios of 0.4, 1.0 and 1.0 (opaque), dried at 60 °C. Key: -□- 0.4/60; -◆- 1.0/60; -■- 1.0/60 (opaque).

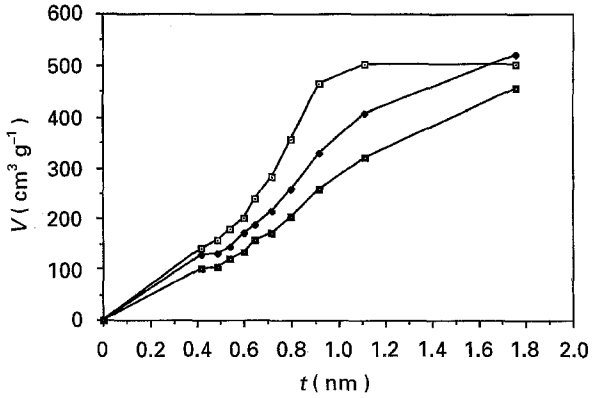

Figure 6 V–t plot of gels prepared with a H_2O/TEOS ratio of 10 and HNO_3/TEOS ratios of 0.4 and 1.0, dried at 120 °C; 0.4 (basic gel) dried at 60 °C. Key: -□- 0.4/120; -◆- 1.0/120; -■- 0.4/60 (basic gel).

differences in both pore size distributions and pore diameters due to the *in situ* formed silica particles.

3.3. V–t plots

The V–t (adsorption volume versus film thickness) curves for the adsorption isotherms of gels prepared in different amounts of acid content at two different drying temperatures are shown in Figs 5 and 6. The 0.4/60, 1.0/60 and 1.0/60 (opaque) gels form a straight line from the origin in the range of low pressure and deviate downward from the straight line at higher pressure are shown in Fig. 5. The adsorption volume of the plateau approximates the micropore volume of the gels. The high acid content gels exhibit a higher micropore volume than those with low acid contents. In Fig. 6, the gels apparently show different V–t curves from the gels in Fig. 5. The curve of the 0.4/120 gel in the beginning shows an upward deviation until P/P_0 of ≈ 0.75 and then heads downward. The curve of the base-aged gel shows an upward deviation from the straight line and starts moving a little downward at higher pressures. A similar feature is also exhibited in an acid-catalysed gel of 1.0/120.

From the slope of the V–t plot, the specific surface area of the gels formed under various conditions are presented in Table I. The results show that the specific

TABLE I Effects of acid content and drying temperature on specific surface areas from V–t Plot

	Drying temperature (°C)			
	60		120	
HNO_3/TEOS ratio	0.4	1.0	0.4	1.0
Specific surface area (m^2/g^{-1})	770	820	526	418

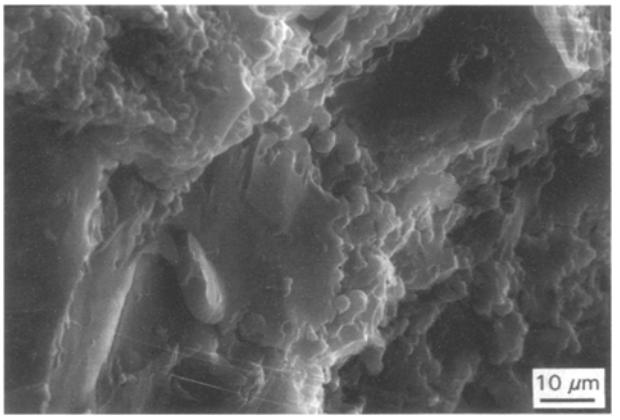

Figure 7 Scanning electron micrographs of fractured surface of gels dried at 60 °C with incorporated precipitates for a H_2O/TEOS ratio of 10 and a HNO_3/TEOS ratio of 1.0.

surface areas increased for gels dried at 60 °C as well as with an increasing HNO_3/TEOS molar ratio in the starting sol. On the other hand, the specific surface areas decreased for gels dried at 120 °C. At a constant acid content, specific surface areas decreased as the temperature increased. The opaque gel has a smaller specific surface area (637 $m^2\,g^{-1}$) than the transparent gel (820 $m^2\,g^{-1}$).

3.4. Microscopic observation

An SEM micrograph of the fractured surface of the gels prepared at a low mixing rate with a H_2O/TEOS ratio of 10 and a HNO_3/TEOS of 1.0 is shown in Fig. 7. It shows that spherical precipitates of 2–5 μm in size formed *in situ* are incorporated in the gel. It appears that the particles in the sol are agglomerated during gelation.

The effect of acid content on the microstructure of the gels dried at 60 °C is shown in Fig. 8. The 0.4/60 gel exhibits homogeneous particles interconnecting the polymeric gel, while the 1.0/60 gel shows a more colloidal gel appearance. Comparison of these micrographs reveals that the pore volume increases with an increasing amount of acid.

Different microstructures for a higher drying temperature of 120 °C are shown in Fig. 9. The 0.4/120 gel shows a homogeneous granular structure constructed of spherical particles 40–130 nm in diameter. The 1.0/120 gel also has a granular structure showing large, loosely packed spherical aggregate which is composed of small particulates. Also, a large space can be seen between the solid phases, indicating an inhomogeneous pore structure. The development of a microstructure by dehydration with heat treatment

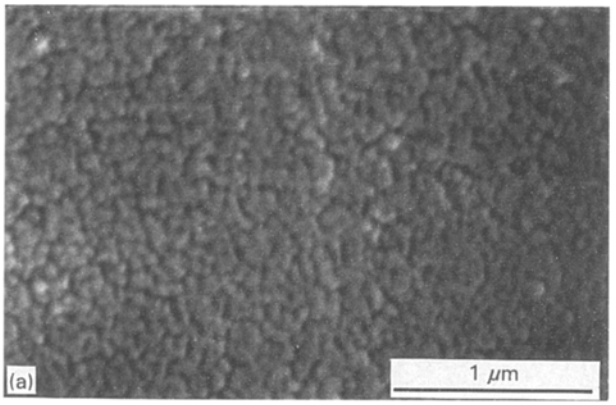

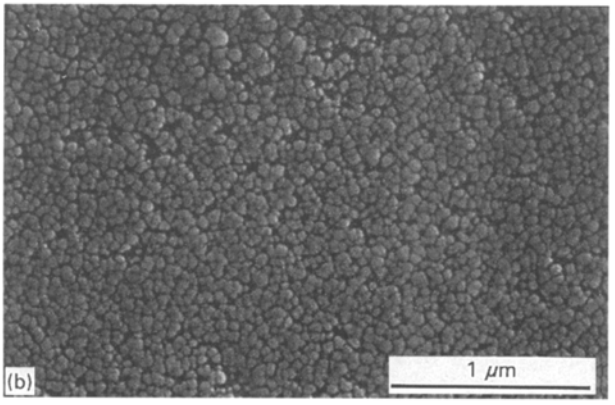

Figure 8 Scanning electron micrographs of fractured surface of gels dried at 60 °C for a H_2O/TEOS ratio of 10 and HNO_3/TEOS ratios of (a) 0.4 and (b) 1.0.

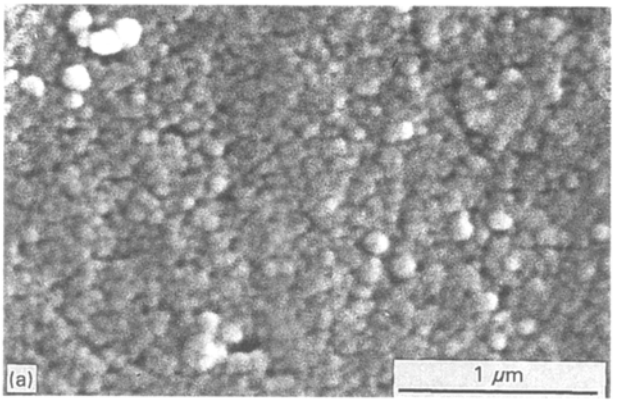

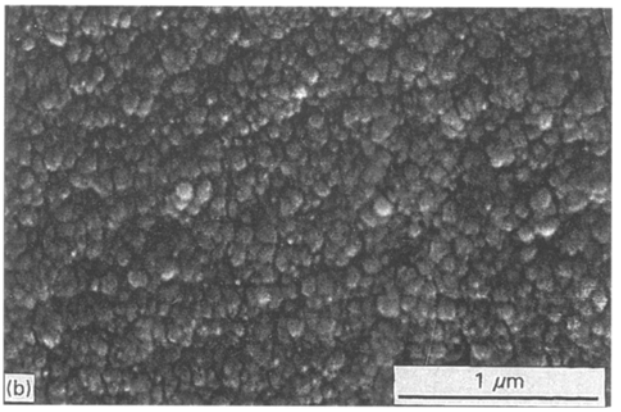

Figure 9 Scanning electron micrographs of fractured surface of gels dried at 120 °C for a H_2O/TEOS ratio of 10 and HNO_3/TEOS ratios of (a) 0.4 and (b) 1.0.

is shown in Fig. 10. The heat treatments bring particles closer together and cause the particles to become further interconnected. The figure shows a considerable decrease in the macroporosity and the particle sizes of agglomerates as the heating temperature is increased.

3.5. FTIR spectra

The Fourier transform infrared (FTIR) spectra of gels before and after the heat treatment at various temperatures are shown in Fig. 11. As shown in all IR spectra of silica gels, characteristic absorption peaks of silicon oxides appeared at around 1070 and 800 cm^{-1}. These correspond to asymmetric and symmetric Si–O–Si stretching vibration modes [12–14]. The spectra also present the 960 cm^{-1} peak assigned to the stretching vibration of Si–OH and 1640 cm^{-1} due to the bending mode of water molecules[11]. In addition to changes in band shape and intensity, it is observed that the absorption at 960 cm^{-1} decreases as the temperature is raised. At the same time, the increase in the absorption at a 1170 cm^{-1} shoulder to 1070 cm^{-1} becomes pronounced. The absorption peaks around 1870 and 1960 cm^{-1} are also enhanced. These peaks are assigned to a combination of various vibration of SiO_2 [15]. It is noted that the absorption peak around 1070 cm^{-1} shifted towards a lower frequency as the absorption of 1170 cm^{-1} shoulder became stronger.

4. Discussion

4.1. Adsorption isotherm and pore size distribution

Pore size distribution or pore structure has a significant role in formation of the bulk gels due to its effect on drying stress distribution. As stated by Lowell and Shields [16], type I isotherms (Fig. 1) are generally observed with porous powder whose pore size does not exceed a few adsorbed molecular layers. This indicates that the gels with type I isotherms have micropores. At high pressure the pores are filled by adsorbed or condensed adsorbate leading to the plateau characteristic of the type I isotherm. Type II isotherms (1.0/120 and 0.4/60 (basic gel) in Fig. 2) most frequently occur for powders with pore diameters larger than micropores. Type IV isotherm (0.4/120 in Fig. 2) is considered to reflect capillary condensation in porous solids with pores in the radius range of an approximately 1.5–100 nm [16].

Plots showing the pore volume of a given pore radius as a function of radius are shown in Figs 3 and 4. The 60 °C-dried gels have narrower pore size distributions than the 120 °C-dried gels. Drying stress developed at the lower drying temperature (60 °C) being larger than that at the higher drying temperature (120 °C) is one likely explanation for this. Generally, the higher the temperature, the lower the surface tension of the contained liquid. Thus, with a lower surface tension the capillary stress decreases. Therefore, pores collapse in low

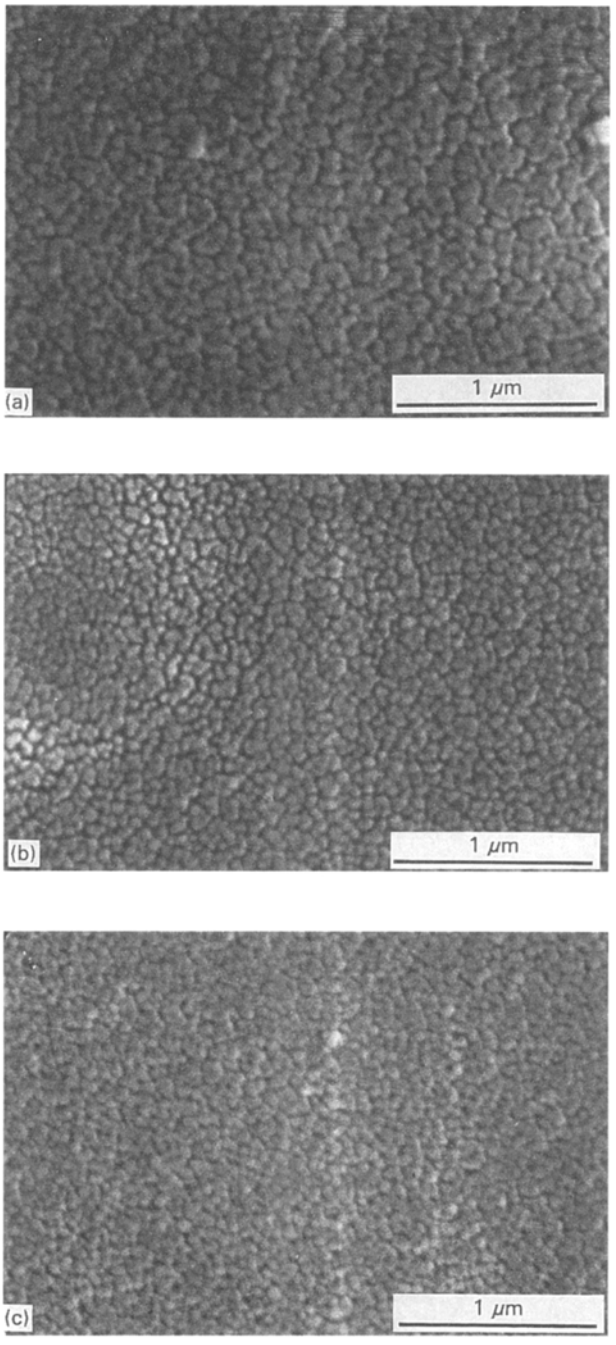

Figure 10 Scanning electron micrographs of fractured surface of gels for a H_2O/TEOS ratio of 10 and a HNO_3/TEOS ratio of 0.4, heat-treated at (a) 200 °C, (b) 400 °C, and (c) 600 °C for 2 h.

temperature gels more easily than in the high temperature gels.

Regarding the effect of acid content on pore size distribution, the differences in sharp and broad pore size distributions between 0.4/60 and 1.0/60 gels can be associated with the gelling time. The longer gelling time of the former results in more regular packing. This leads to a sharper pore size distribution. This also holds true for the gels of 0.4/120 and 1.0/120. At high acid concentration with high ionic strength, the zeta potential on the sol particles becomes low due to the compressed double layer. This then results in a decrease of the gelling time.

As for the 120 °C-dried gels, increasing acid content increases the pore radii, broadens the pore size distribution, and increases the pore volume. These results

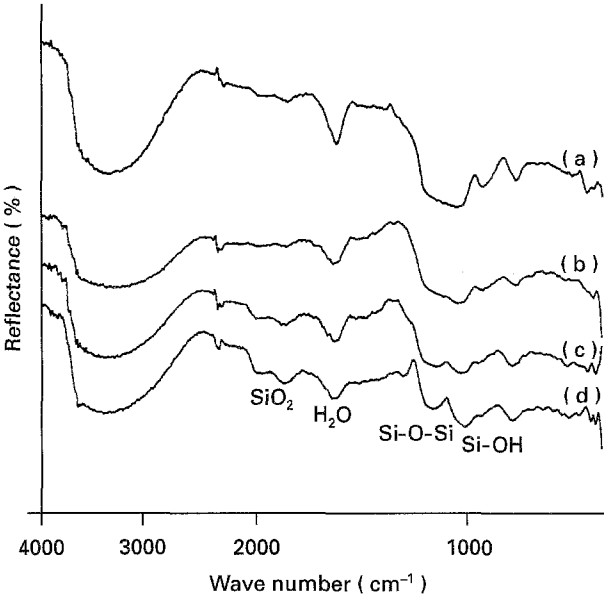

Figure 11 FTIR spectra of silica gel for a H_2O/TEOS ratio of 10 and a HNO_3/TEOS ratio of 0.4 as function of heating temperature at (a) 60 °C, (b) 200 °C, (c) 400 °C, and (d) 700 °C.

lead to lower surface areas with larger pore sizes. However, for the 60 °C-dried gel with a narrow pore size distribution, increasing the acid content increased the pore volume. This resulted in higher surface areas with smaller pore sizes.

There was no notable difference in the pore size distribution and pore size between gels with and without the presence of silica particles. This suggests that the *in situ* formed silica particles have a pore structure similar to that of the gel itself but a somewhat smaller total pore volume as shown in Fig. 1.

4.2. Pore structure

Lippens and deBoer [10] have shown that valuable information on the pore structures may be obtained by plotting the volume of adsorbed nitrogen (V) as a function of the layer thickness of the adsorbed nitrogen (t) according to previous isotherms. The straight line goes through the origin. Its slope is a measure of surface area. Three types of V–t curves were distinguished and explained by Lippens and deBoer [10]:

1. For the straight line with a constant slope, the surface is freely accessible up to high relative pressure; the multilayer can be formed unhindered on all parts of the surface in the absence of any pore filling.
2. For a upward deviation from a straight line, the material takes up more adsorbate than the corresponding volume of the multilayer. This means that at a certain pressure, capillary condensation will occur in larger pores of cylindrical shape.
3. For a downward deviation from a straight line, no capillary condensation can occur in slit-shaped pores. At a certain relative pressure the pores may be completely filled by the adsorbed layers on both parallel walls, thereby reducing the available surface for continued adsorption.

From Fig. 5, the V–t curves of 0.4/60 and 1.0/60 gels are classified as the third type according to the Lippens and deBoer model. This indicates that the gels dried at 60 °C, regardless of the amount of acid used, have slit-shaped pores with small pore sizes as shown in Fig. 3. However, the 0.4/120, 1.0/120 and basic gels shown in Fig. 6 evidently have a completely different pore structure. For the 0.4/120 gel, the V–t curve indicates that the gel has relatively wide pores with narrow openings. This is referred to as the ink-bottle shape. The openings themselves are formed by slit-shaped pores [15]. On the other hand, the curve of the 1.0/120 gel indicates that the gel has wide pores with larger openings. Therefore, drying at 120 °C gives a larger apparent pore size than drying at 60 °C. Furthermore, reactions occurring in an even higher acid content from molar ratio of 0.4 to 1.0, enlarge the opening of the pores. This phenomenon is apparent from the SEM micrographs in Figs 8 and 9.

4.3. Gel microstructure

As shown in Fig. 7, the tendency of particulate agglomeration in the gel is probably due to the unstable particles formed in the sol during the reaction. The ionic strength of the sol is made very high by the high concentration of nitric acid. This compresses the thickness of the double layer of the sol particle surface. The decreased thickness of double layer results in a reduction of repulsive forces between particles, and enhances the agglomeration of particles. In addition, the sudden burst of nucleation under the high acid condition yields a fast growth of precipitates until the concentration of nuclei reaches below the supersaturation level.

A comparison of the SEM micrograph of the 60 °C-dried gel (Fig. 8) with that of the 120 °C-dried gel (Fig. 9), reveals that the slightly larger particles for the latter is from the higher drying temperature. A higher temperature leads to greater silica solubility. This allows the primary particles to grow through Ostwald ripening [16]. Thereby, particles grow in size and decrease in number as highly soluble small particles dissolve and reprecipitate on larger, less soluble nuclei. This is shown in Table I as a decrease in the specific surface area.

The effects of acid content and drying temperature on microstructures are evident from the pore size distributions (Figs 3 and 4) and the SEM micrographs (Figs 8 and 9). A narrow pore size distribution and homogeneous particle size are observed on 0.4/60 and 0.4/120 gels. However, a wider pore size distribution and less homogeneous particle sizes are shown in 1.0/60 and 1.0/120 gels. The difference in pore size distribution can be associated with the gelling time. As the gelling time increases ($R_a = 0.4$), the particles have more time to rearrange themselves and lead to more regular packing. Therefore, a narrow pore size distribution is obtained. The uniform pore size, and the narrow size distribution along with the formation of homogeneous particle size promote the formation of bulk dried gels without cracking. During drying, an uneven stress occurs due to varying evaporation rates caused by the non-uniform pore sizes.

In Fig. 10, as the heat treatment temperature increases, the macroporosity and the particle sizes of the agglomerate decreases. This is due to the further condensation that increases the overall connectivity and density. The increasing connectivity results in a reduction in aggregate size due to the decreased micropores in aggregates, and an increase in the oxide content of the molecule. This is confirmed by FTIR results discussed below that show a higher ratio of bridging oxygen with an increase in oxide content.

4.4. FTIR spectra

The chemical changes with heat treatment for the gels of low acid content is observed. The decrease in the IR absorption at 960 cm^{-1} in Fig. 11 is attributed to the decrease in the amount of SiOH due to the dehydration condensation of silanols. It disappears at around 700 °C, showing that most of the silanols have been spent in dehydration condensation by this temperature. The spectra show strong absorption at 1170 cm^{-1} due to Si–O–Si vibration characteristics of the spectra of pure vitreous silica [13]. As heat treatment temperature increases the 1170 cm^{-1} peak becomes prominent. The appearance of absorptions at 1960, 1870 and 1170 cm^{-1}, and the diminishing at 960 cm^{-1} indicate the formation of SiO_2, resulting in an increase of the oxide content. As to the shift of 1070 cm^{-1} peak toward a lower frequency, Lippincott *et al.* [15], in their infrared study on polymorphs of silicon oxide, explained the shift as the change in angle that the tetrahedral units make with each other.

5. Conclusions

1. By increasing drying temperature, the pore structure significantly changes to larger pore size and broader pore size distribution. At a constant drying temperature, however, the higher acid content gives a higher pore volume.
2. From the results of pore size and its distribution and V–t plot, the 0.4/60 and 1.0/60 gels have slit-shaped micropores with narrower pore size distribution. Whereas, the 0.4/120 and 1.0/120 gels have ink-bottle shaped pores with a relatively broad size distribution.
3. The pore size distribution and SEM results show that the 0.4/60 and 0.4/120 gels have more homogeneous microstructures than those 1.0/60 and 1.0/120 gels.

References

1. M. GUGLIELMI and G. CARTURAN, *J. Non-Cryst. Solids* **100** (1988) 16.
2. C. J. BRINKER and G. W. SCHERER, in "Ultrastructure Processing of Ceramic Glasses and Composites", edited by L. L. Hench and D. R. Ulrich (Wiley, New York, 1984) p. 43.
3. C. J. BRINKER, *J. Non-Cryst. Solids* **100** (1988) 31.

4. A. YASUMORI, H. KAWAZOE and M. YAMANE, *ibid.* **100** (1988) 215.
5. J. ZARZYCKI, M. PRASSAS and J. PHALIPPOU, *J. Mater. Sci.* **17** (1982) 3371.
6. J. ZARZYCKI, in "Ultrastructure Processing of Ceramic Glasses and Composites", edited by L. L. Hench and D. R. Ulrich (Wiley, New York, 1984) p. 27.
7. L. C. KLEIN and G. J. GARVEY, in "Ultrastructure Processing of Ceramic Glasses and Composites", edited by L. L. Hench and D. R. Ulrich (Wiley, New York, 1984) p. 88.
8. L. L. HENCH, in "Science of Ceramic Chemical Processing", edited by L. L. Hench and D. R. Ulrich (Wiley, New York, 1986) p. 52.
9. K. T. CHOU and B. I. LEE, *Ceram. Int.* **19** (1993) 315.
10. B. L. LIPPENS and J. H. deBOER, *J. Catal.* **4** (1965) 319.
11. S. BRUNAUER, L. S. DEMING, W. S. DEMING and E. TELLER, *J. Amer. Chem. Soc.* **62** (1940) 1723.
12. A. BERTOLUZZA, C. FAGNANO, M. A. MORELLI, V. GOTTARDI and M. GUGLIELMI, *J. Non-Cryst. Solids* **48** (1982) 117.
13. M. PAUTHE, J. PHALIPPOU, R. CORRIU, D. LECLERCQ and A. VIOUX, *ibid.* **113** (1989) 21.
14. G. ORCEL, G. J. PHALIPPOU and L. L. HENCH, *ibid.* **88** (1986) 114.
15. E. LIPPINCOTT, A. V. VALKENBURG, C. E. WEIR and E. N. BUNTING, *J. Res. Nat. Bur. Stand.* **61** (1958) 61.
16. S. LOWELL and J. E. SHIELDS, "Powder Surface Area and Porosity" (Chapman and Hall Ltd, New York, 1984) p. 11.
17. C. J. BRINKER and G. W. SCHERER, "Sol-Gel Science, the Physics and Chemistry of Sol-Gel Processing" (Academic Press Inc., New York, 1990) p. 524.

Received 2 June 1994
and accepted 16 August 1995